Analysis and Application of Coal Seam Seismic Waves for detection of Abandoned Mines

Daniel Jackson Yancey

Thesis submitted to the Faculty of the
Virginia Polytechnic Institute and State University
in partial fulfillment of the requirements for the degree of

Master of Science
in
Geosciences

Dr. Matthias G. Imhof, Chair
Dr. John A. Hole
Dr. J. Arthur Snoke

May 1, 2006
Blacksburg, Virginia

Keywords: Coal Seam, Dispersion, Guided Waves, Mining Geophysics, Seam Waves, Void Detection

Analysis and Application of Coal Seam Seismic Waves for detection of Abandoned Mines

Daniel J. Yancey

ABSTRACT

It is not uncommon for underground coal mining to be conducted in the proximity of abandoned underground mines that are prone to accumulate water, methane or other toxic gases, and are often either poorly mapped or without good surface survey control. Mining into such abandoned voids poses a great safety risk to personnel, equipment, and production from inundation or toxic/explosive gas release. Often, surface or underground drilling is employed to detect the mine void and evaluate the hazards, sometimes with disastrous results. Guided waves within coal seams can be utilized to locate voids, faults, and abrupt seam thickness changes. Another application of guided waves is mine planning.

To demonstrate the feasibility of abandoned mine void detection utilizing coal seam seismic waves, two in-seam reflection surveys and one transmission survey were acquired at an abandoned underground mine near Hurley, Virginia. The field surveys were complemented by numerical modeling. The dominant Airy phase was observed in the synthetic and field data. Dispersion analysis of the field data shows reasonable agreement with the dispersion characteristics of the synthetic data. Using standard commonly available seismic reflection processing tools, the well mapped demonstration mine was detected and located with an accuracy better than 50 m from a distance of 400 m.

Detection of the mine with both surveys indicates that "exploratory" drilling can be replaced by noninvasive seismic methods. Location, however, may not be good enough to replace drilling entirely. We conclude that seismic methods can be used for detection, but if a potential void is detected, focused drilling should be applied for accurate mapping and circumvention of potentially hazardous areas.

Acknowledgments

I owe a great deal of thanks to a number of people who have assisted me with my project. My advisor, Dr. Matthias Imhof, has proven to be an invaluable resource during my studies. I deeply appreciate his continuing patience and assistance regarding my development as a scientist. Dr. J. Arthur Snoke has always provided assistance as well as been an outlet for any questions or ideas I might have and also provided me with his dispersion analysis program *mfilt*. Dr. John Hole has also played a vital role in my development as a scientist and researcher during my tenure, and I extend my sincerest gratitude to him. Dr. Martin Chapman was a great resource in helping me understand dispersion characteristics of seam waves. Richard Godbee always provided time to answer any technical questions I had and I thank him. Tod Gresham and John Feddock (Marshall Miller & Associates), two of my colleauges with whom we collaborated with on this project, were valuable resources as well. TECO Energy provided access to the mine site. I thank the Mine Safety and Health Administration for providing funding for the study. The creators of Computer Programs in Seismology (Herrmann, 2004), Seismic Analysis Code (Goldstein et al., 2003) and The Generic Mapping Tools (Wessel and Smith, 1991) have my thanks. Everyone who participated in the field data collection has my sincerest thanks.

My office mates and friends at Virginia Tech have been a tremendous help. I owe thanks to Elige Grant, Ryan Lester, and Jiedi Wu for insightful discussions about our projects and great friendships. Arvind Sharma has provided continuous help and support throughout my career here and I greatly appreciate his friendship. Dave Loveday has provided me with a great friendship as well. I owe tremendous thanks to Ankit Singhal for his help and friendship during this past year.

Throughout my life my family has provided me with unwavering support and love. Without their love and encouragement, I wouldn't be where I am today, and I thank them for that.

By far, my upmost thanks goes to God for giving me all the opportunities I have been presented in my life. It is to Him that I owe everything.

Contents

List of Figures

List of Tables

Chapter 1

Introduction

It is not uncommon for underground coal mining to be conducted in the proximity of abandoned underground mines, which are prone to accumulate water, methane or other toxic gases. Often, they are either poorly mapped, or are without good surface survey control. Mining into such abandoned mine voids poses a great risk to personnel safety, equipment, and production from inundation or explosive gas release. The mining disaster at Quecreek, PA in 2002, is a prime example. While operating underground, nine miners were trapped by water underground when they accidentally cut into old mine workings. The old workings had filled with water that rushed through the gap and trapped the miners underground. Fortunately these miners were rescued, but this may not always be the case.

The standard method for detecting abandoned voids utilizes drilling over the selected area with a specific grid pattern optimized to increase the probability of intercepting a potential void. However, room and pillar methods can only extract 30–45 % of the coal, leaving roughly 60 % of the coal underground to support the roof. Drilling into one of these pillars gives no indication that the area has been previously mined or not. Acoustic seam waves trapped in the coal seam, however, can be utilized for void detection. Seam waves can be used to detect and locate perturbations in coal seams, such as faults, pinchouts, or mined-out underground voids (Buchanan et al., 1981; Mason et al., 1980). To test the In-Seam Seismic (ISS) method for void detection, two ISS reflection surveys and one transmission survey were acquired at a temporarily abandoned mine near Hurley, Virginia (Figure 1.1).

The Sassy No. 1 Mine, owned by TECO Energy, was selected to demonstrate void detection and location because it is well-mapped with known outlines. Furthermore, it has both water and air-filled sections which allows demonstration of detection under different conditions. ISS methods were used because, unlike surface geophysical methods, they are independent of surface conditions such as rough topography and directly target the area of interest.

Reflected seam waves can be used to map the coal-void interface. The seam wave will propagate through the coal seam, strike the void interface, and travel back to the receiver array at the coal face (Figure 1.2). Imaging of reflected seam waves can not only be used for void detection, but also for mine planning, such as fault and pinchout detection.

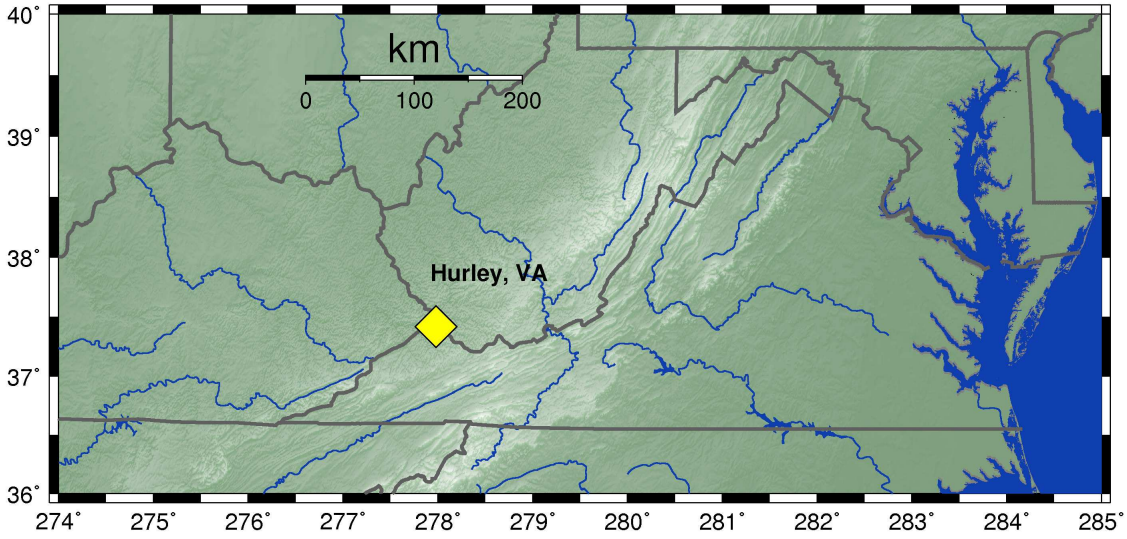

Figure 1.1: Location Map of Study Area. Shading indicates topography.

Evison (1955) and Krey (1962) first noted dispersed wavetrains on seismograms recorded in underground mines. They showed analytically that the low impedance coal seam acts as a waveguide, effectively trapping seismic energy with propagation predominantly within the seam. Mason et al. (1980) used reflection ISS to image a fault cutting through a coal seam. Buchanan et al. (1981) used both reflection and transmission ISS for fault detection. The data processing sequence for seam waves however, is less developed than for reflection surface seismics. Mason et al. (1980) and Buchanan et al. (1981) proposed two imaging methods: dynamic trace gathering (DTG) and adaptive lag sums (ALS).

Dynamic trace gathering is a generalization of normal moveout (NMO) corrections employed on surface seismic reflection data. Because the reflecting interface may not be necessarily parallel to the source-receiver line, the assumption of reflection at the common midpoint (CMP) cannot be made. Instead, a range of reflector orientations are systematically tested. For each midpoint, traces with source-receiver combinations that satisfy angle of incidence equals angle of reflection with this particular reflector orientation are selected, moveout corrected and stacked. The moveout correction is not necessarily symmetric as it is generally assumed for surface reflection seismics. At each CMP and time, the stack from the orientation that yields the largest magnitude is selected for the image. This procedure is not used for the processing of surface reflection data, and hence, is not included in common data processing packages. Buchanan et al. (1981) used the adaptive lag sum algorithm, which is similar to conventional Kirchhoff prestack depth migration currently used routinely in seismic data processing (Yilmaz, 1987). An additional complication is the dispersive nature of the seam waves, which demands that each frequency of the seam wave be processed and imaged separately. Mason et al. (1980) proposed the usage of wavelet compressors to render

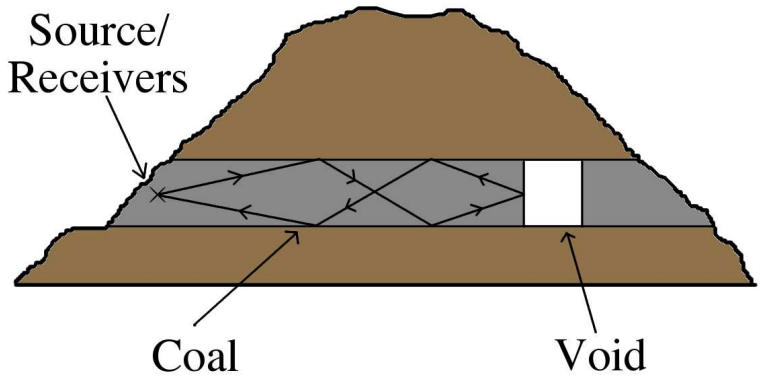

Figure 1.2: Cross section example of void detection.

the dispersed wavetrains more pulse-like.

Instead of redeveloping specialized algorithms, we opted for using tools contained in common reflection seismic processing packages. The wavetrains were not compressed, but instead, the amplitude traces were converted to envelope traces using the Hilbert transform (Dombrowski et al., 1994). Lastly, we replaced dynamic trace gathering or adaptive lag sums with conventional Kirchhoff prestack depth migration. Nevertheless, we obtained images which allow not only detection of mine voids, but also estimation of their locations.

Chapter 2

Theory

Channel or seam waves form in coal seams as a result of the physical properties of coal and the embedding country rock. Coal is typically a low-density rock ($\approx$ 1300 kg/m^3) that is sandwiched between denser formations, such as sandstone and shale with densities exceeding 2000 kg/m^3. Moreover, the rocks directly above and below the seam often exceed the seismic P- and S- wave velocities in coal by a factor of two (Dombrowski et al., 1994). The P-wave velocity of coal ranges from 1600 m/s to 2400 m/s, while the S-wave velocity ranges from 700 m/s to 1400 m/s (Dombrowski et al., 1994). Hence, the acoustic impedance ratio, the product of velocity and density, can exceed four to one.

The low-velocity coal seam acts as a seismic waveguide with modes strongly excited for sources placed within the seam. The impedance contrast at the upper and lower boundaries of the coal seam causes strong reflections. For a source in the seam, the result is multiply reflected energy bouncing between the seam boundaries (Figure 2.1). For near vertical propagation, with angles of incidence smaller than the critical angle, the reflection is sub-critical, and energy will be transmitted through the seam boundary into the surrounding rock. These are known as leaky modes. For near horizontal propagation with angle of incidence exceeding the critical angle, the energy is reflected with little transmission into the surrounding rock forming normal modes or seam waves. For every frequency, constructive interference occurs at a different horizontal wavenumber, and hence, seam waves are typically dispersive. In practice, this model is complicated by the fact that seam waves can be formed by constructive interference of P-, SV-, SH-, head, and interface waves. This constructive interference causes local minima and maxima for the group velocity and forms large amplitude arrivals known as Airy phases (Aki and Richards, 2002).

Two independent types of seam waves form when the critical angles at the seam boundary are exceeded. The first type is a SH (or "Love-type") seam wave, also referred to as an *Evison wave* 1955, whose particle motion is horizontal and transverse to the direction of P-, SV-propagation. The second type of seam wave is a *Krey wave* (pseudo-Rayleigh wave Krey, 1962) that forms by interference of P- and SV- waves with particle motion in the vertical-longitudinal plane. Even pure P or S sources may excite seam waves due to the coupling at the boundaries. A coal seam face near the source furthers the formation of seam waves by

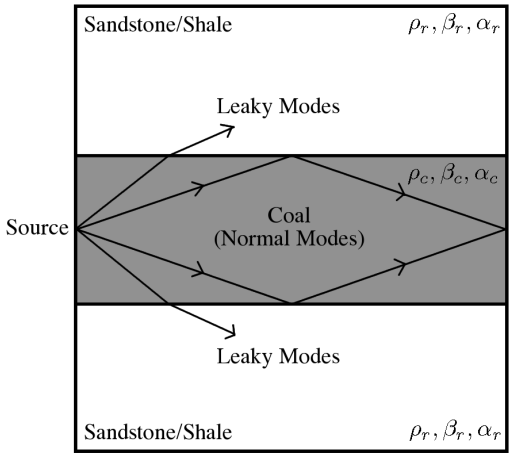

Figure 2.1: Development of guided coal seam waves

mode conversion.

Evison (1955) and Krey (1962) found that seam waves are dispersive: different frequencies propagate at different speeds. The result is the broadening of an initially spiky signal into an extended wavetrain. Dombrowski et al. (1994) showed that Krey and Evison waves have phase velocities bound between the shear wave velocities of the coal and the surrounding rock. Regueiro (1990) demonstrated that the amplitudes of the seam waves are large inside coal but decay rapidly in the floor and roof.

If a propagating seam wave encounters any perturbation in the waveguide, it will be reflected predominantly as a seam wave, although some energy may be scattered as body waves. Such seam perturbations can be caused by voids, faults, or abrupt pinchouts. Hence, reflection of seam waves can be used to detect voids and potentially map their location and outline.

Chapter 3

Data Acquisition & Processing

The Splashdam coal seam is a flat-lying seam in the Appalachian Plateau of Virginia with an approximate thickness of 75 cm and a thin shale parting of 4 cm as shown in Figure 3.1. The Sassy No. 1 mine is located near Hurley, Virginia and is owned by a subsidary of TECO Energy. Mining operations began in November 2001, but were suspended in December 2002. Since then, the low-laying areas of the mine have been filling with water. A map of the mine is presented in Figure 3.2. Although the mine is underground, the coal seam outcrops in nearby river valleys allowing access to test seismic detection of the known mine. One in-seam transmission survey was acquired, as well as two in-seam reflection surveys. Performing the demonstration surveys in the open allowed easy access and working conditions as opposed to working in cramped underground spaces.

The objectives of the transmission survey were independent identification of seam waves and the estimation of velocities and dispersion using a simple, controlled geometry. The objectives of the reflection surveys were to demonstrate detection and location of the mine under different conditions. Using a bulldozer and a bucket excavator, an existing bench and seam outcrop was cleared to allow for unrestricted access for placement of the seismic equipment. Along the outcrop, weathered country rock and coal were removed to obtain a clean face exposing fresh coal (Figure 3.3).

The transmission survey consisted of a 15 m long receiver array with 30 geophones at 0.5 m spacing. We used 100 Hz vertical geophones, but mounted them perpendicular to the face of the seam outcrop by drilling a hole with a 6 mm diameter into the seam and driving the geophone spike into it with a rubber hammer. Normally, vertical geophones should not be mounted horizontally, but the stiff springs in the high frequency geophones permit this usage. For seismic sources, we used a sledgehammer striking a railroad spike placed in the seam inside the mine at two locations, located at distances of 170 m and 220 m from the receiver array. The spike was struck ten times at each location. Each hit was recorded separately for later stacking to increase the signal to noise ratio. Transmission survey parameters are summarized in Table 3.1.

Two reflection surveys were also acquired. Table 3.1 lists the line parameters for each reflection survey. ISS Line 1 is located near the water-filled section of the mine, while ISS

Figure 3.1: Splashdam Seam, Hurley, Virginia.

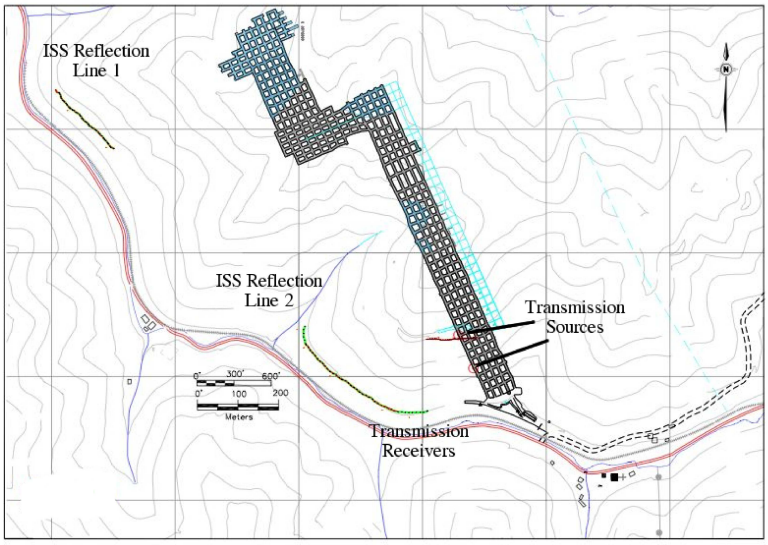

Figure 3.2: Sassy No. 1 Mine Layout.

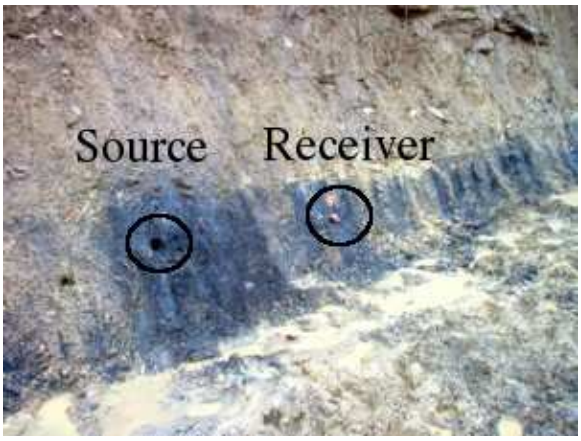

Figure 3.3: Source/Receiver installation on coal outcrop.

Line 2 is near the air-filled section (Figure 3.2). For the seismic sources, we used explosive charges of 0.15 kg placed in holes drilled 1 to 1.5 m into the seam. The holes were drilled far enough to prevent fracturing or cracking of the face. After placing the charge, each hole was carefully tamped with gravel to maximize coupling and radiation of seismic energy. Figure 3.3 shows the seam with source boreholes and receivers.

3.1 Data Processing: ISS Transmission Survey

The transmission data were analyzed to identify seam wave events and to estimate their velocity. Predictive deconvolution with a lag of 16.6 ms was applied to remove pervasive 60 Hz powerline noise. The gathers of each source point were then stacked to increase the signal to noise ratio. Figure 3.4 presents transmission seismograms clearly showing seam waves. The velocity of the Airy phase of the fundamental mode was determined to be 490 m/s.

3.2 Data Processing: ISS Reflection Surveys

The same processing sequence was applied for both in-seam reflection surveys using the Promax processing software. First, a bandpass filter was applied to remove low frequency groundroll and high frequency noise. True amplitude correction was performed to account for geometrical spreading. The data were badly contaminated by 60 Hz powerline noise because coal mining equipment in nearby mines is operated on electric power. Predictive deconvolution was used to remove this periodic powerline noise. Figure 3.5 shows a shot gather from ISS Line 1 after bandpass filtering, deconvolution and true amplitude recovery has been applied. The dispersed reflected seam wave arrival is clearly visible at ≈ 0.8 seconds. The strong airwaves were removed by automated surgical muting and further manual mutes were applied to remove direct body and surface waves. Automatic gain control was then

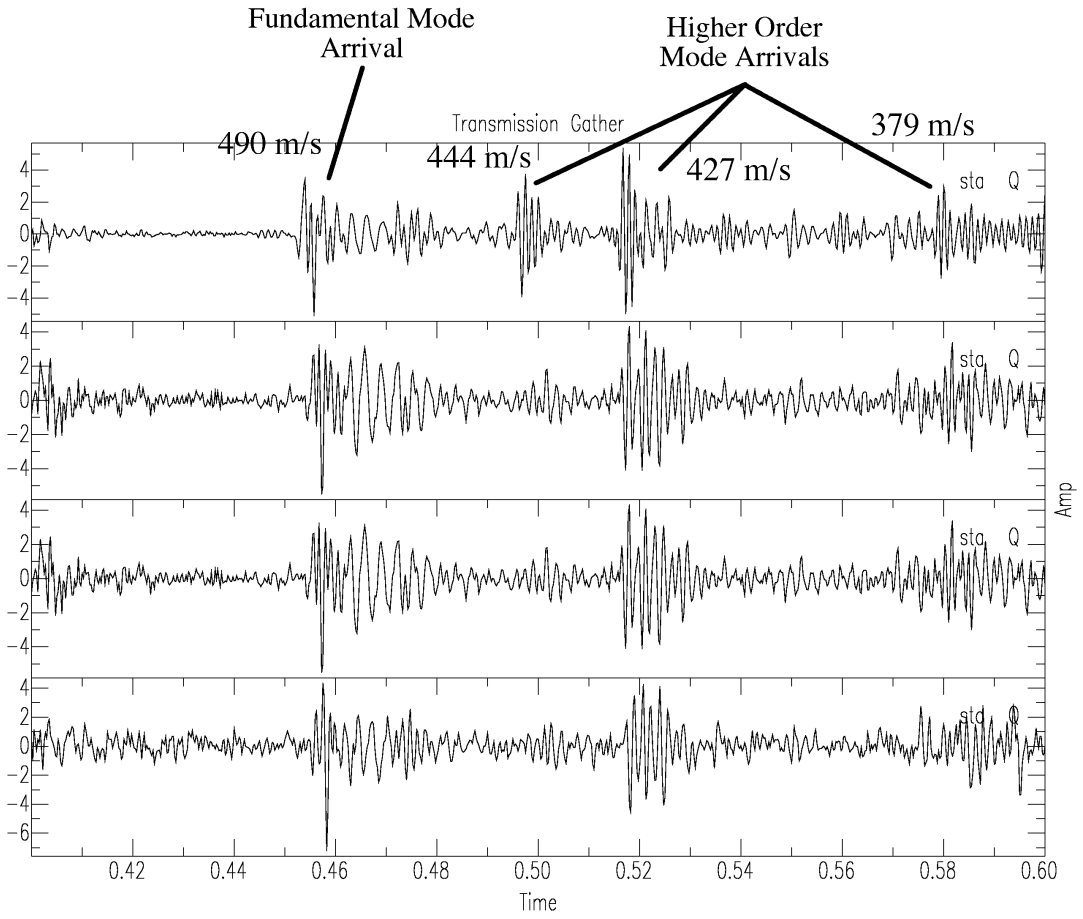

Figure 3.4: Recorded data from transmission survey of the Splashdam seam at Hurley, VA

Parameters	Transmission	ISS Line 1	ISS Line 2
Sources	2	37	47
Shot Spacing	50 m	3.5 m	6.0 m
Usable Shots	20	36	39
Channels	30 (100 Hz)	60 (100 Hz)	60 (100 Hz)
Receiver Spacing	0.5 m	3.5 m	3.0 m
Total Line Length	15 m	210 m	365 m
Sample Rate	0.25 ms	0.25 ms	0.25 ms
Recording Length	1.0 s	5.0 s	5.0 s
Source Hole Depth	0.0 m	1.0 m	1.0 m
Source Size	hammer, 10 blows	0.15 kg	0.15 kg
Target Distance	170 and 220 m	380 m	240 m

Table 3.1: In-Seam Transmission and Reflection Survey Parameters

applied to balance the remaining data and enhance higher order mode arrivals. Instead of dispersion compression (Mason *et al.*, 1980), the amplitude traces were transformed to envelope traces (Figure 3.6). Envelope formation ensures that constructive interference will occur when the gathers are stacked, even with slightly wrong velocities. If the envelopes are not used and no other measures are taken, destructive interference can occur. The dispersive wavetrains with a duration of $\approx 20\ ms$ were thus transformed to ≈ 50 Hz wavelets exhibiting positive amplitudes only. Given the low velocity, this reduction in frequency and resolution does not hamper the survey objectives.

Instead of redeveloping the earlier imaging methods (Buchanan et al., 1981), conventional 2-D Kirchhoff prestack depth migration was used for imaging. Migration is assumed to be in depth. The ISS Reflection surveys, however, require lateral imaging. To reduce imaging artifacts, the geometry was rotated 90 degrees along a horizontal axis chosen to approximate the crooked geometry best. Traditional 2-D depth was replaced by the plane of the coal seam and inline distances, while topography was replaced by the curvature around the contour of the seam outcrop. The velocity model for the migration was a constant velocity of 490 m/s as determined from the transmission survey. To examine the effects of velocity model errors, models with constant velocities in the range of 440 m/s and 540 m/s ($\pm 10\%$) were tested. These tests all showed the same mine reflectors with comparable sharpness, albeit with slightly different distances from the outcrop. The migrated shot gathers were stacked to obtain a final image.

Figure 3.7 shows the stacked image for Line 1. According to the mine plans, the true distance from the seam face to the void is 380 m. The strongest reflection is observed at a distance close to 380 m. Similar results were obtained for Line 2 presented in Figure 3.8. According to the mine plans, the true distance to the void is between 210 m and 310 m because the outcrop and mine boundary are at an angle. A coherent event is seen in Figure 3.8 at the expected location. While location is not as good for Line 2, detection of the

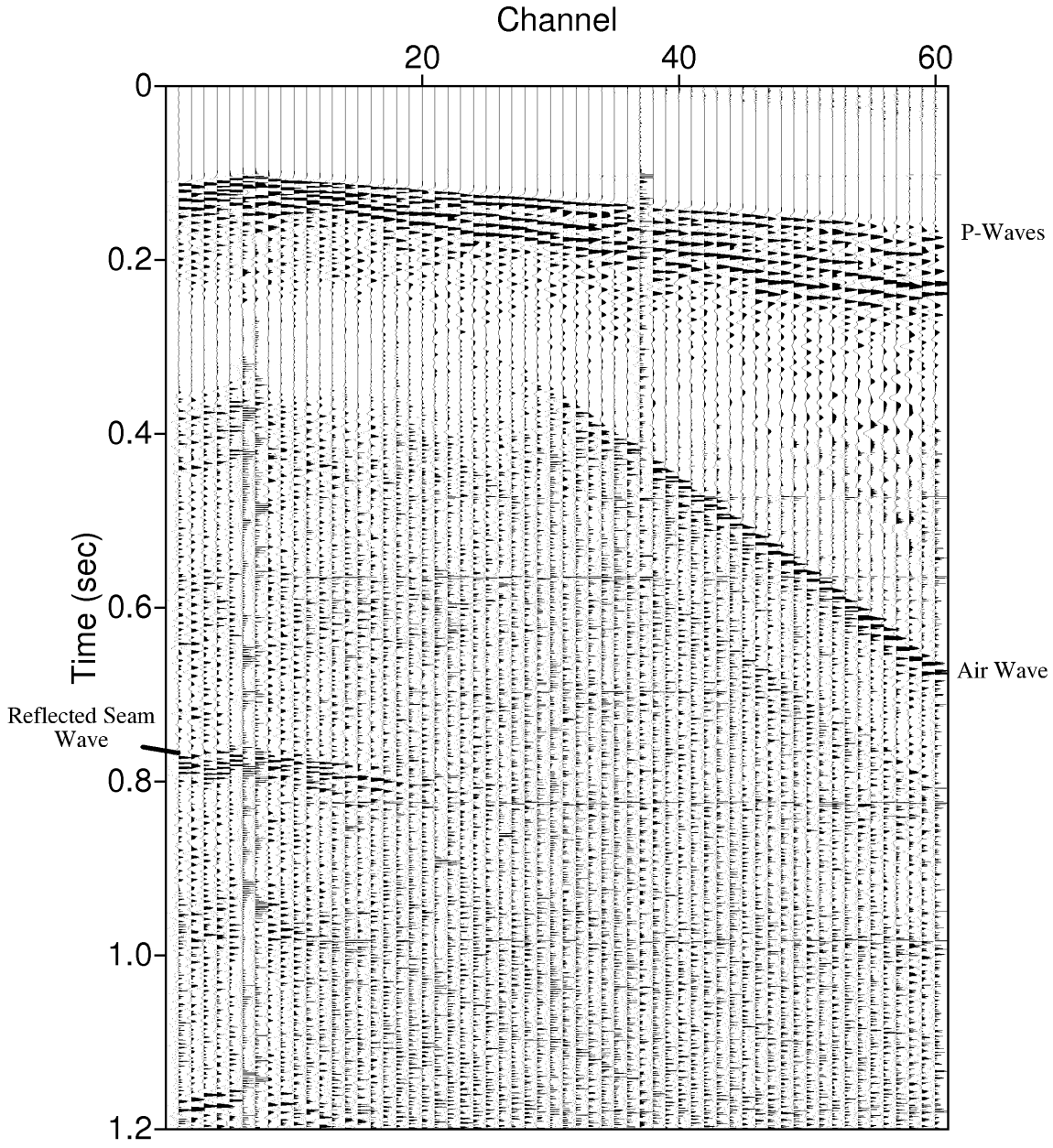

Figure 3.5: Shot gather from ISS Reflection Line 1 after pre-processing.

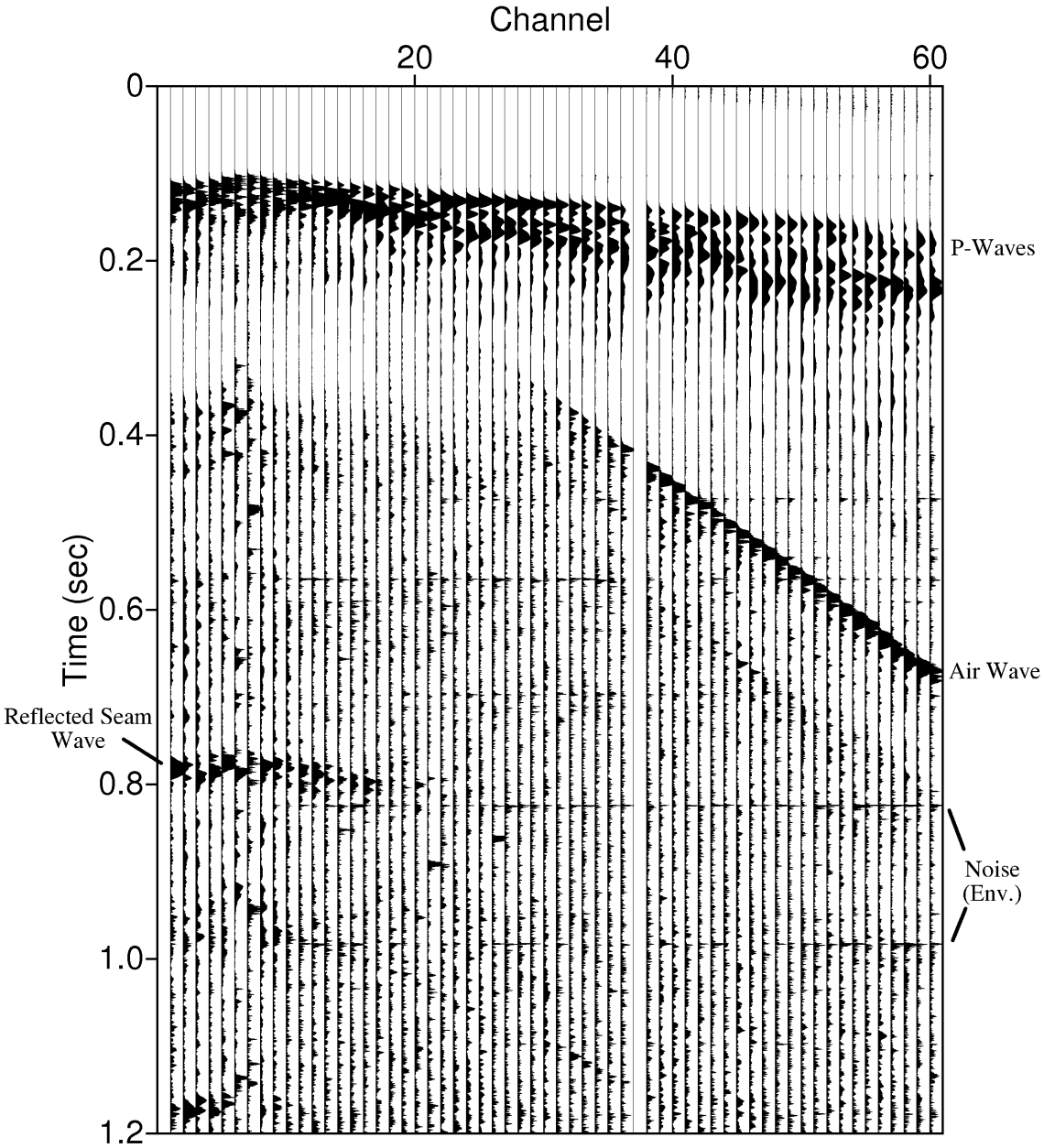

Figure 3.6: Shot gather shown in Figure 3.5 after envelope formation to convert the dispersed wavetrains into simpler events suitable for migration.

abandoned mine is still straightforward.

Figures 3.9 and 3.10 show plan views of the mine site with interpreted horizontal seismic sections from Figures 3.7 and 3.8 overlaid and scaled to the size of the map. Figure 3.9 shows that while the ISS Reflection Line 1 seismic projection is not directly in-line with the mine, an event can still be seen near the correct location of the mine. The abandoned mine for Line 1 has numerous diffractors (labeled A, B and C) and yet has coherent reflectivity. Figure 3.10 shows the same view for ISS Reflection Line 2. The western edge departs slightly from the correct location of the mine. A large number of misfires occurred near this area and resulted in a loss of shots, and thus, near-offset traces which tend to contain the best and strongest seam wave events as demonstrated in Figure 3.5. To image dipping reflectors, a large migration aperture is required. The survey line would need to extend farther to the northwest. However, from the eastern edge of the section to the middle portion, the interpreted line is at the correct location of the mine-void interface. No shots were lost, data coverage was better, and hence, migration worked better.

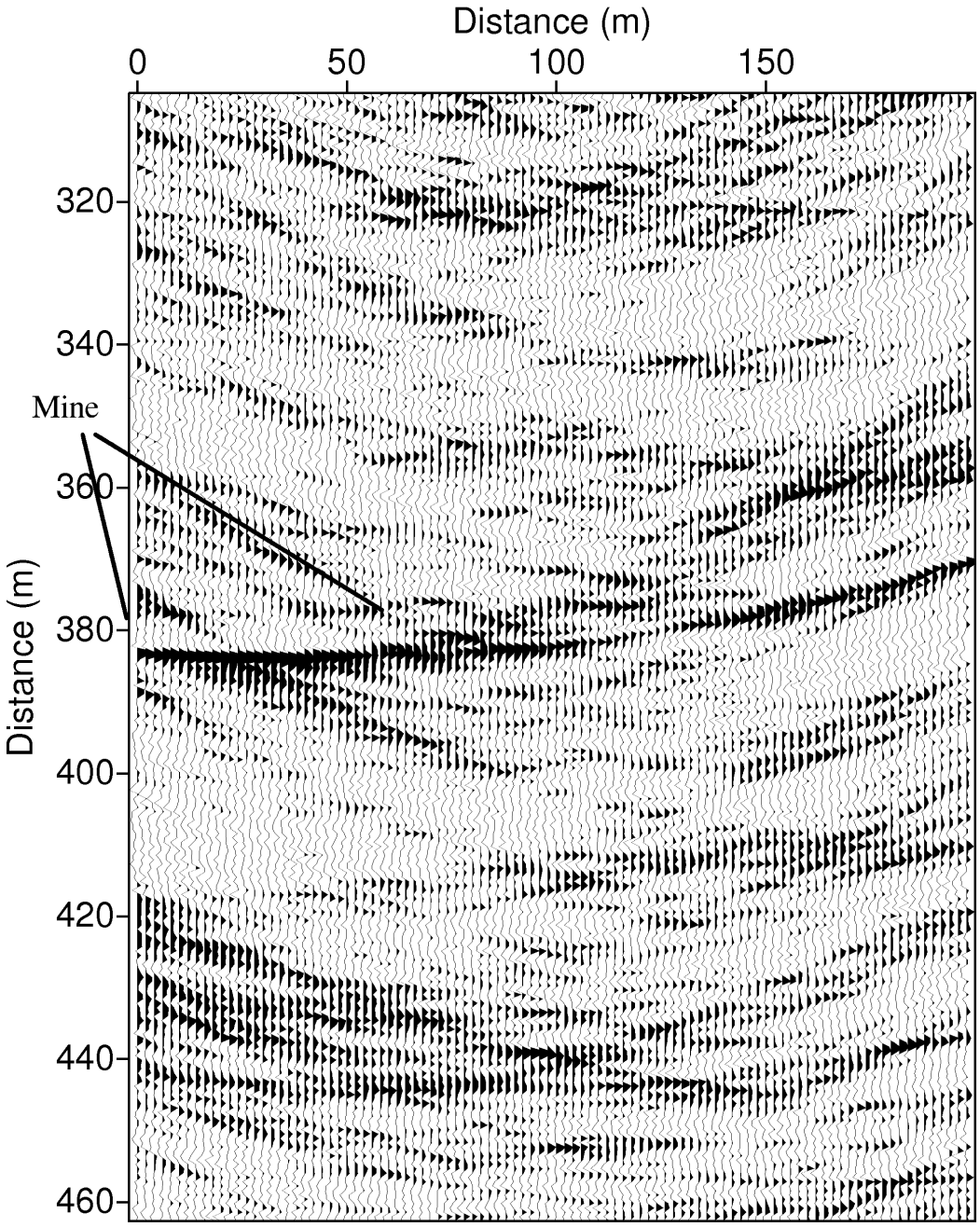

Figure 3.7: Stacked ISS Reflection Line 1 results. The first 60 m of the section are the part of the event which is interpreted as the mine reflection.

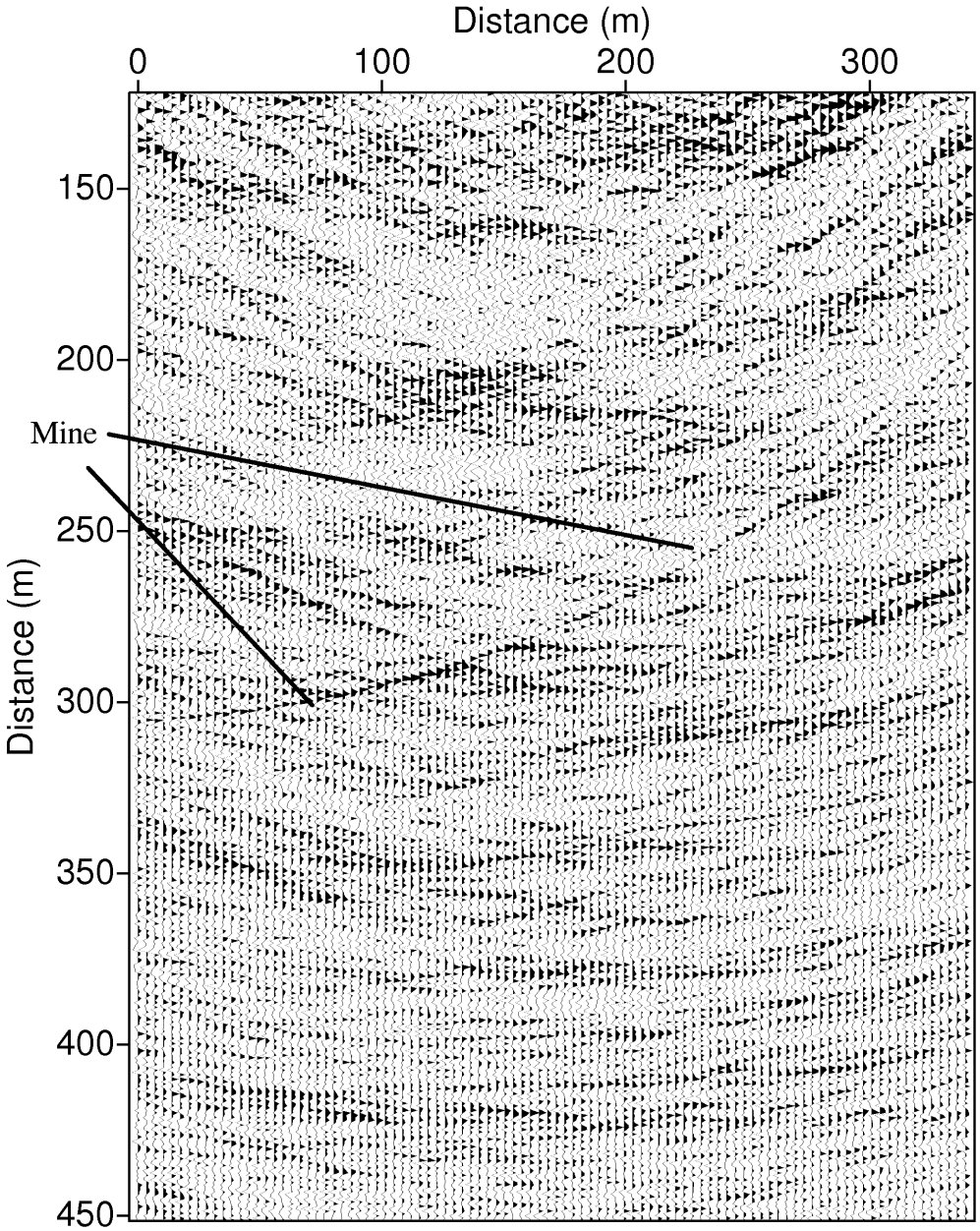

Figure 3.8: Stacked ISS Reflection Line 2 results. The black bars indicate the part of the event which is interpreted as the mine reflection.

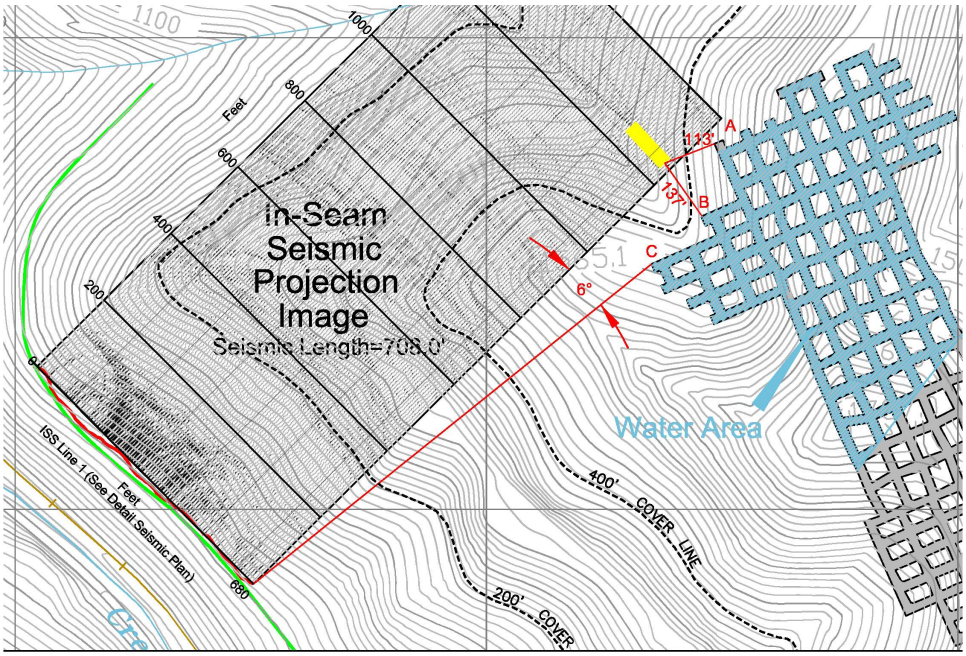

Figure 3.9: Results of overlaying ISS Reflection Line 1 on the map. The projection shows that the location of the seismic event is very close to the actual mine-void boundary. Yellow line is the interpreted portion of the seismic section in Figure 3.7.

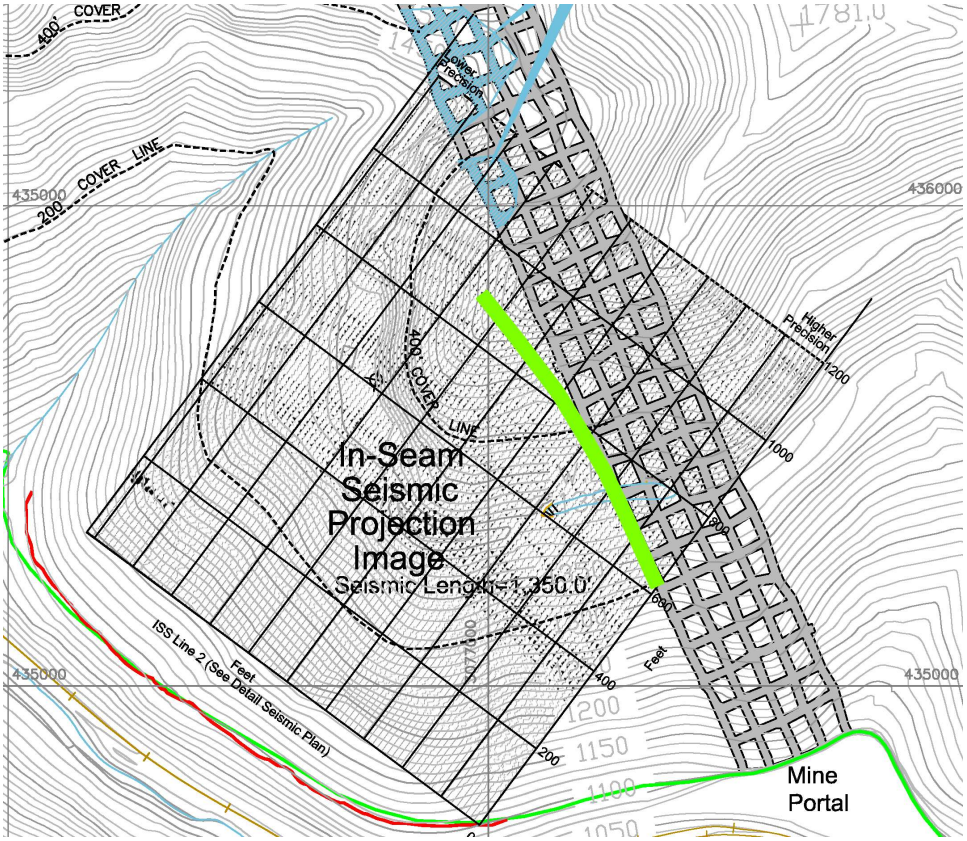

Figure 3.10: Results of overlaying ISS Reflection Line 2 on the map. Location towards the eastern edge of the mine is good while departure is seen towards the western end as a result of poor aperture. Green line denotes the interpreted portion of the seismic section in Figure 3.8.

Chapter 4

Numerical Modeling & Dispersion Analysis

Numerical modeling of the transmission survey geometry was performed for comparison between synthetic data and the recorded field data. Lacking in-situ measurements, values for V_p, V_s, and ρ were estimated from published data (Dombrowski et al., 1994). All computations were performed using the Computer Programs in Seismology (CPS) modeling package (Herrmann, 2004). First, analytical solutions for the phase and group velocities of the Love and pseudo-Rayleigh type seam waves were computed using an analytical root finder (Herrmann's sdisp96 program). Second, synthetic seismograms were computed by numerical wavenumber integration where the hammer source was modeled by a horizontal force (Herrmann's hspec96 program). Appendix C gives sample flowcharts for both the analytical solution and wavenumber integration. Three simple 1-D layerstack models were created to approximate the conditions at the demonstration site.

This analysis required building a layerstack of the coal seam sequence, source and receiver descriptors, as well as source-receiver offsets. The workflow can be generalized as follows:

Each model has a different stacking pattern (Figures 4.1-4.3): $rock_1/coal/rock_1$ (symmetric), $rock_1/coal/rock_2$ (asymmetric) and $rock_1/coal/dirtband/coal/rock_1$ (embedded dirtband). P- and S- wave velocities are denoted by the subscripts p and s respectively, the impedance by I and the density by ρ. The subscripts r1, r2, c, and d denote values for $rock_1$, $rock_2$, *coal* and *dirtband* respectively. The parameter values for each of these models are given in Table 4.1.

1. A layerstack model consisting of P- and S- wave velocities, densities and thicknesses is defined by the user for all layers.

2. A numerical root finder solves the dispersion equation to determine group and phase velocities.

3. The Green's functions for the layerstack model are calculated for the desired source and receiver locations.

	$rock_1$ $coal$ $rock_1$	$rock_1$ $coal$ $rock_2$	$rock_1$ $coal/dirt/coal$ $rock_1$
V_{pr1} (m/s)	2000	2000	2000
V_{sr1} (m/s)	1400	1400	1400
ρ_{r1} (kg/m^3)	2200	2200	2200
I_{pr1} (kg/sm^2)	4400000	4400000	4400000
I_{sr1} (kg/sm^2)	3080000	3080000	3080000
V_{pr2} (m/s)	-	1600	-
V_{sr2} (m/s)	-	900	-
ρ_{r2} (kg/m^3)	-	1900	-
I_{pr2} (kg/sm^2)	-	3040000	-
I_{sr2} (kg/sm^2)	-	1710000	-
V_{pc} (m/s)	1200	1200	1200
V_{sc} (m/s)	700	700	700
ρ_c (kg/m^3)	1300	1300	1300
I_{pc} (kg/sm^2)	1560000	1560000	1560000
I_{sc} (kg/sm^2)	910000	910000	910000
V_{pd} (m/s)	-	-	1300
V_{sd} (m/s)	-	-	900
ρ_d (kg/m^3)	-	-	1600
I_{pd} (kg/sm^2)	-	-	2080000
I_{sd} (kg/sm^2)	-	-	1440000

Table 4.1: P and S wave velocities (denoted by subscripts p and s), impedances and densities for the three layerstack models. Subscripts r1, r2, c and d denote values for $rock_1$, $rock_2$, *coal* and *dirtband* respectively. Velocities and densities obtained from Dombrowski et al. (1994).

4. The source spectrum and the Green's function are multiplied in the frequency domain and converted into the time domain by the Fourier transform.

4.1 Dispersion Analysis of the Wavenumber Integration Technique Results

For the wavenumber integration, the synthetic trace that most accurately described our transmission survey setup was the transverse component for a horizontal point force (THF) (Radial components for all seam models can be found in Appendix A). Figure 4.4 shows all synthetic THF traces for the three types of coal seam sequences. A very well developed

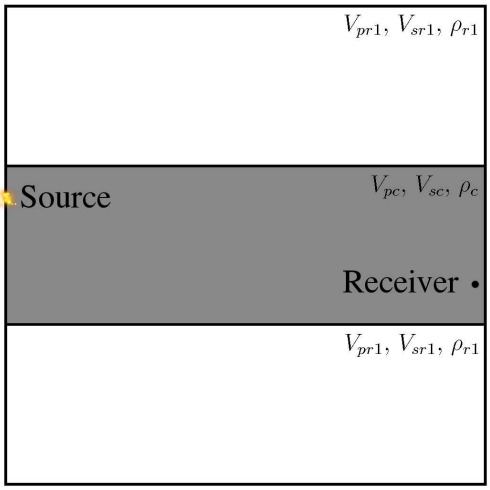

Figure 4.1: Layerstack model for symmetric coal seam sequence.

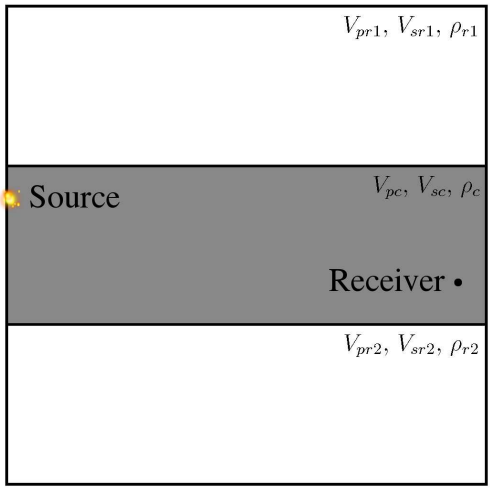

Figure 4.2: Layerstack model for asymmetric coal seam sequence.

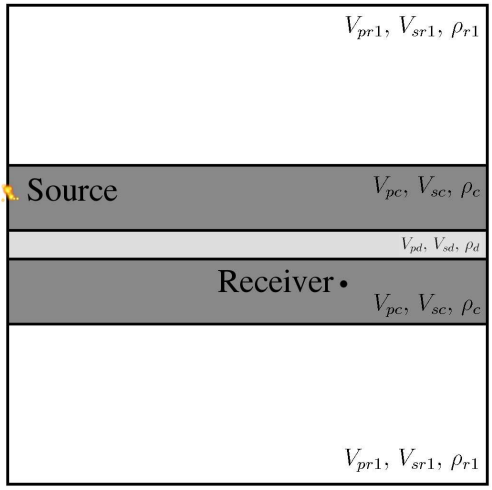

Figure 4.3: Layerstack model for embedded dirtband coal seam sequence.

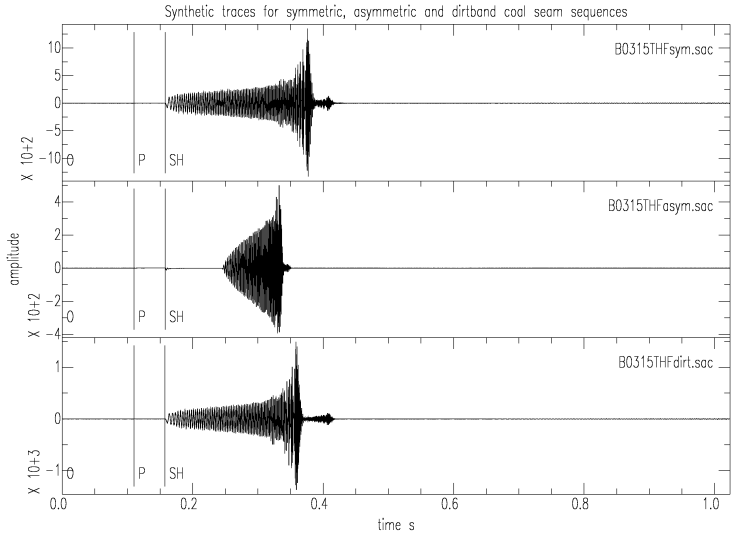

Figure 4.4: Synthetic traces for symmetric (top), asymmetric (middle) and embedded dirtband coal seam sequences (bottom).

dispersed wavetrain starts to arrive at about 0.15 seconds for the symmetric and embedded dirt band sequences. The dispersed wavetrain arrives later for the asymmetric case. In addition, near 0.35 seconds, an arrival with a very large amplitude is seen for all three cases which is interpreted as the Airy phase (Aki and Richards, 2002). Airy phases are associated with extrema, typically minima, of the group velocity. Dispersion analysis of these events support this interpretation.

Figures 4.5, 4.6 and 4.7 show the results of the multiple filter technique (MFT) applied to the synthetic seam waves in Figure 4.4. The program *mfilt* by Snoke was used for this analysis (Snoke and James, 1997). This program is based on Dziewonski et al. (1969), but incorporates enhancements including instantaneous frequency and the display enhancing filter by Nyman and Landisman (1977).

Contours on each of the dispersion plots indicate the highest 20 % amplitude values. As described above, the long periodic portion of the dispersed wave is seen earlier in the seismic trace, and hence has a faster group velocity. For all seam sequences, the large amplitude Airy phase is seen arriving last with frequencies of 700–1000 Hz and with a group velocity range of 500–600 m/s.

4.2 Analytical Solutions for Coal Seam Waves

Analytical solutions for the Love and pseudo-Rayleigh coal seam waves were also computed using a numerical root solver to solve the dispersion equation for phase and group velocities

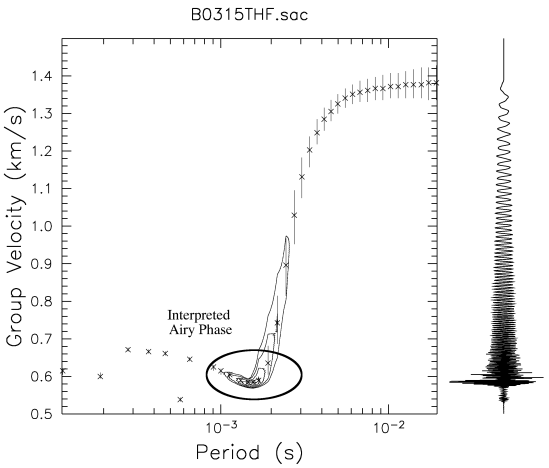

Figure 4.5: Dispersion Analysis of synthetic trace for symmetric coal seam sequence. Contours indicate the top 20 % of amplitude values.

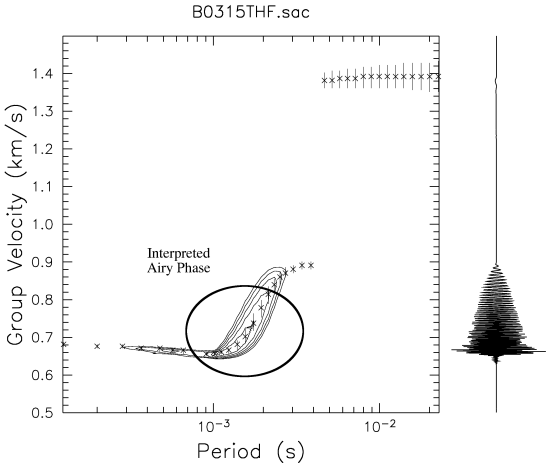

Figure 4.6: Dispersion Analysis of synthetic trace for asymmetric coal seam sequence. Contours indicate the top 20 % of amplitude values.

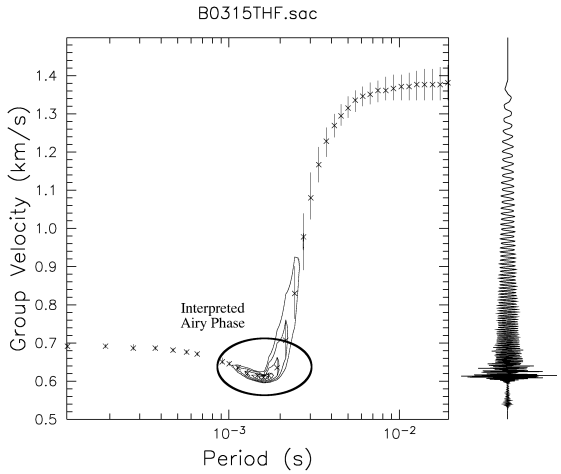

Figure 4.7: Dispersion Analysis of synthetic trace for embedded dirt band coal seam sequence. Contours indicate the top 20 % of amplitude values.

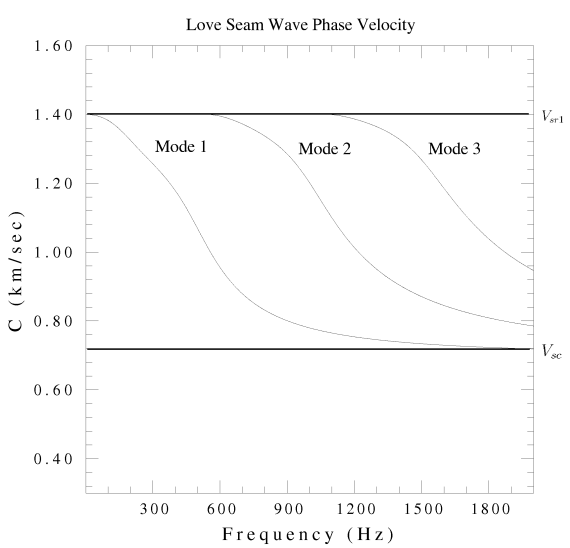

Figure 4.8: Analytical solution for the Love type seam wave phase velocity for first three modes. Phase velocities are bound between shear wave velocities of the coal (V_{sc}) and surrounding rock (V_{sr1})(dark horizontal lines shown in plot).

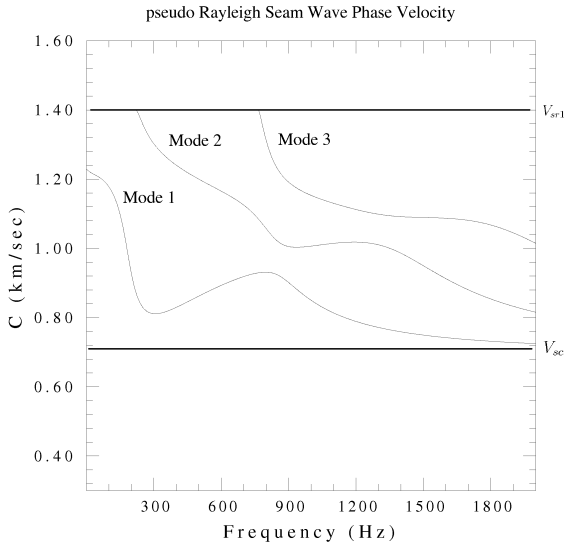

Figure 4.9: Analytical solution for the pseudo-Rayleigh type seam wave phase velocity for first three modes. Phase velocities are bound between shear wave velocities of the coal (V_{sc}) and surrounding rock (V_{sr1})(dark horizontal lines).

(Herrmann, 2004). The same layerstack models were used as for the wavenumber integration. Figures 4.8 and 4.9 show the phase velocities for the first three modes for the Love and pseudo-Rayleigh seam waves. Dombrowski et al. (1994) showed that the phase velocities for the coal seam waves are bound between the shear velocities of the coal and surrounding rock. Figures 4.8 and 4.9 confirm these bounds. Both the Love and pseudo-Rayleigh seam waves have phase velocities for all three modes that are bound between the shear velocities of the surrounding rock and coal.

Seismic events, however, propagate with the group velocity, not the phase velocity. Figures 4.10 and 4.11 show the group velocities for the Love and pseudo-Rayleigh seam waves. The Airy phase arrivals (denoted by A) for the Love type seam wave drop below the shear wave velocity of the coal. Similar results are obtained for the pseudo-Rayleigh seam wave. There are many present for the pseudo-Rayleigh seam wave that are above or below the shear wave velocity of the coal.

4.3 Dispersion Analysis of Transmission Survey

Figure 3.4 showed four traces extracted from the transmission survey at a distance of 220 m. Very nicely developed arrivals are seen at 0.46 seconds (fundamental mode arrival), and at 0.50, 0.52 and 0.58 seconds (higher order mode mode arrivals).

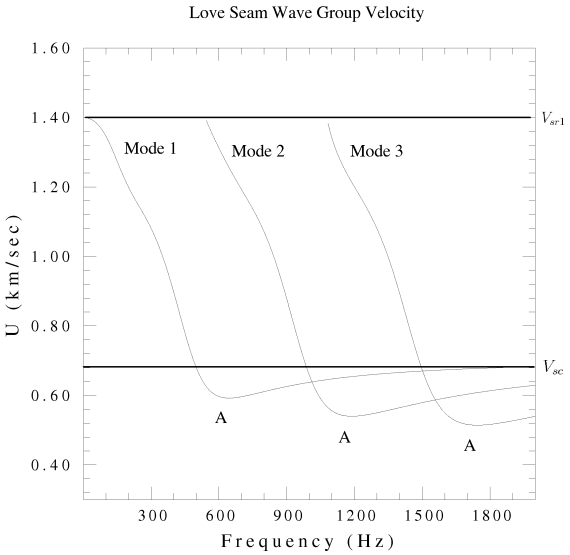

Figure 4.10: Analytical solution for the Love type seam wave group velocity for first three modes with interpreted Airy phases.

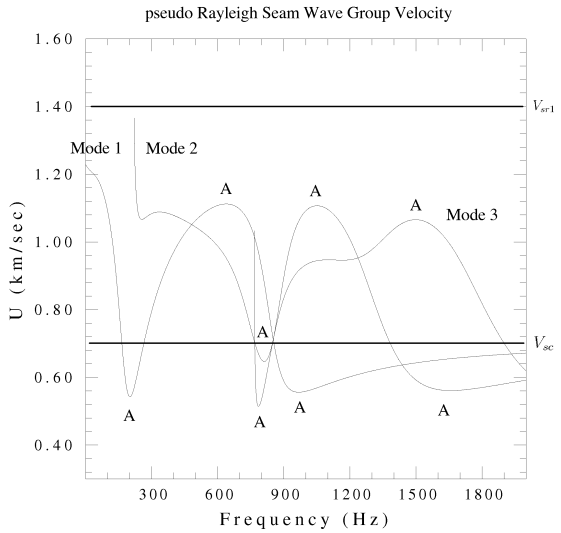

Figure 4.11: Analytical solution for the pseudo-Rayleigh seam wave group velocity for first three modes with interpreted Airy phases.

Dispersion analysis of the traces were carried out for comparison with the synthetic results. Figure 4.12 shows the dispersion analysis for one selected trace. Contours indicate the highest 20 % of amplitude values. The initial longer periodic portion of the seam wave is observed, followed by a large amplitude arrival. The frequency range for the interpreted Airy phase is between 700–1100 Hz with a group velocity range of 400–550 m/s. These results agree reasonably well with analytic solutions and wavenumber integration techniques for Airy phase arrivals.

4.4 Discussion of Dispersion Analysis of Field Data and Numerical Models

With the geometry of geophones mounted perpendicular to the face of the coal seam, the Love seam wave is expected to be recorded more so than the pseudo-Rayleigh seam wave because the seam outcrop where the geophones were placed is subparallel to the line of sight from the source locations (Figure 3.2). If the geophones were mounted at an angle, one would obtain recordings for both the Love and pseudo-Rayleigh seam waves. Interestingly, the fundamental mode arrival seen for all traces in Figure 3.4 shows a very short duration, higher frequency arrival, followed immediately by a lower frequency arrival over a time interval of ≈ 0.02 seconds. The group velocity analytical solution for the Love seam wave shows three Airy phases with comparable group velocities and frequencies that reasonably correspond to the observed data. Also present in the field data are higher modes with increasing frequency

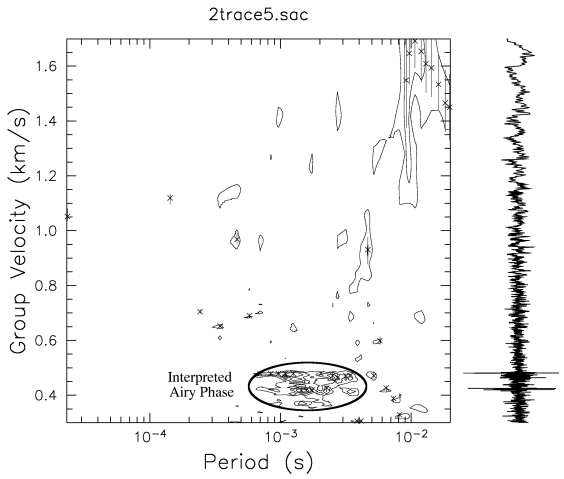

Figure 4.12: Dispersion Analysis of record data at Hurley, VA. Contours indicate the highest 20 % amplitudes.

content for each Airy phase arrival and a slower group velocity. These observations are consistent with the analytical solutions for either the Love or pseudo-Rayleigh seam wave group velocities. The fundamental mode arrivals and subsequent higher order mode arrivals for both the Love and pseudo-Rayleigh seam waves have very comparable group velocities. Hence, it is quite possible to have both the Love and pseudo-Rayleigh seam wave arrivals in the same data, although enhancement of the Love type seam wave is expected. ISS Line 1 should contain predominantly the pseudo-Rayleigh seam wave reflections, while ISS Line 2 should have reflections from both types of seam waves due to the angle between the coal seam outcrop and the mine-void interface. Since both the Love and pseudo-Rayleigh seam waves have comparable group velocities, imaging with either type using a small range of velocities ($\pm$10% of 500 m/s) should be reasonable. In fact, we may have migrated a combination of both types.

The Airy phase for the fundamental mode of the coal seam wave is observed in both synthetic modeling and recorded data. The synthetic coal seam waves computed by wave number integration show well developed dispersion for the entire length of the trace with the Airy phase in a frequency range of 700–1000 Hz and a group velocity of 500–600 m/s. The analytical solutions for the Love and pseudo-Rayleigh seam waves indicate existence of multiple Airy phases, and modes, with a comparable group velocity and frequency range for the fundamental mode as seen in the recorded data. Compared to the wavenumber integration results, the field data do not show an equally well dispersed wavetrain for the coal seam wave, although the large amplitude Airy phase is observed with a similar range of frequencies (700–1100 Hz) and with a comparable group velocity (400–550 m/s) for both types of seam waves.

Chapter 5

Discussion

The presented results demonstrate that in-seam seismic methods can be used for detection of abandoned mines. Standard and widely available seismic tools and software can be used for data acquisition and processing. The acquisition parameters of in-seam surveys have a significant impact on the detectability and imaging of mined-out areas. Long lines allow mapping of greater portions of the mine boundary. Dense seismic arrays will result in better detectability and mapping of voids. Single-component high-frequency vertical geophones can be mounted perpendicular to the face of the coal seam. Although not demonstrated, multicomponent geophones might improve the results and allow utilization of both Rayleigh and Love seam waves for void location and detection. Different types of sources can be used. For distances up to at least 200 m, a hammer source proved to be adequate for generating detectable one-way transmission seam waves. For distances up to 500 m, charges of 0.15 kg were sufficient for generating seam waves used for reflection detection and imaging. Although not tested, other sources, such as a shotgun or piezoelectric source, should perform equally well. The seam outcrop needs to be clean and ideally present a fresh surface with no significant cracking or fracturing for good coupling. This demonstration survey was performed at a surface outcrop, but the approach should allow extension to void detection in the advance of mining in underground seam faces. If no surface outcrop of the seam exists, then underground usage would be ideal.

If reasonable estimates of compressional and shear wave velocities for the site can be obtained beforehand, reliable estimates of the Airy phase group velocity of both the Love and pseudo-Rayleigh seam waves can be calculated for multiple modes. Otherwise, a transmission survey is needed. The transmission survey could have source and receiver geometries consisting of face-face, face-borehole, or borehole-borehole combinations inside the mine or at an outcrop. The distance between source and receiver should be large enough to allow the development of the Airy phase and separation from other arrivals. A short distance of 150 m was tested, but less could possibly suffice. The seam waves were easy to identify on seismic data.

The processing sequence for in-seam reflection surveys is summarized in Table 5.1. Removal of powerline noise was accomplished by predictive deconvolution. The bandpass filter

should pass all frequencies associated with the anticipated fundamental and higher order mode arrivals (typically 400–1200 Hz). High amplitude air blast and other undesired phases are removed by automated and surgical muting. Cylindrical divergence associated with geometric spreading of the wavefront can be corrected by true amplitude recovery. The wavelet compression used by Buchanan et al. (1981) and Mason et al. (1980) can be replaced with envelope formation without substantial loss of spatial resolution. Previously used custom imaging techniques can be replaced with 2-D Kirchhoff prestack depth migration now commonly available in standard seismic data processing toolboxes.

In-Seam Seismic Reflection Workflow
Load Geometry
Trace Edit
Bandpass Filter
Predictive Deconvolution (60 Hz removal)
True Amplitude Recovery
Air Blast Mute
Mute direct energy
Automatic Gain Control
Envelope Formation
Kirchhoff Prestack Depth Migration
Stack migrated gathers

Table 5.1: ISS Reflection Processing Workflow

The detectability of voids also depends on data coverage and aperture. The location accuracy of the detected void depends upon the velocity estimate of the Airy phase arrival. The location accuracy along the survey line depends both on velocity and data coverage. An often used rule of thumb is that the lateral location uncertainty is on the order of a Fresnel zone after migration. With a velocity estimate of 490 m/s, the Fresnel zone is about 50 m at a distance of 305 m and 70 m at a distance of 610 m. The detection of voids is independent of the type of mine fill, as both air and water-filled sections were detected. Fault detection and location was performed by Buchanan et al. (1981) and Mason et al. (1980). Although not tested, collapsed roof (gob) can also potentially be detected.

Chapter 6

Conclusions

The in-seam seismic method is very applicable for detecting mine voids or other geologic perturbations in a coal seam. Both acquisition and processing can be executed using standard tools used for surface seismic surveys. A processing workflow was developed which replaces custom processing algorithms with ones now contained in virtually all commercial or public domain seismic data processing systems. Voids in a seam are relatively easy to detect, but location is not accurate enough to be used as the sole means of mine planning. The in-seam method should be accurate enough, however, to replace exploratory drilling for mine void detection with drilling targeted specifically to areas where mine voids were seismically detected ideally reducing the cost of drilling.

Bibliography

Aki, K., and Richards, P., 2002, Quantitative Seismology: University Science Books.

Buchanan, D., Davis, R., Jackson, P., and Taylor, P., 1981, Fault location by channel wave seismology in united kingdom coal seams: Geophysics, **46**, 994–1002.

Dombrowski, B., Dresen, L., and Rüter, H., 1994, Seismic coal exploration Part B: In-seam seismics: Elsevier Science Inc. Tarrytown, NY.

Dziewonski, A., Bloch, S., and Landisman, M., 1969, A technique for the analysis of transient seismic signals: Bulletin of the Seismological Society of America, **59**, 427–444.

Evison, F., 1955, A coal seam as a guide for seismic energy: Nature, **176**, 1224–1225.

Goldstein, P., Dodge, D., Firpo, M., and Minner, L., 2003, Sac2000: Signal processing and analysis tools for seismologists and engineers: Invited contribution to The IASPEI International Handbook of Earthquake Engineering Seismology.

Herrmann, R., 2004, Computer programs in seismology-an overview of synthetic seismogram computation, version 3.30: St. Louis University http://www.eas.slu.edu/People/RBHerrmann/CPS330.

Krey, T., 1962, Channel waves as a tool of applied geophysics in coal mining: Geophysics, **28**, 701–714.

Mason, I., Buchanan, D., and Booer, A., 1980, Fault location by underground seismic survey: Institution of Electrical Engineers, **127**, 322–336.

Nyman, D., and Landisman, M., 1977, The display-equalized filter for frequency-time analysis: Bulletin of the Seismological Society of America, **67**, 393–404.

Regueiro, J., 1990, Seam waves: What are they?: The Leading Edge, **19**, 19–23.

Snoke, J., and James, D., 1997, Lithospheric structure of the Chaco and Paraná basins of South America from surface-wave inversion: Journal of Geophysical Research, **102**, 2939–2951.

Wessel, P., and Smith, W., 1991, Free software helps map and display data: Eos Transactions, AGU, **72-41**, 445–446.

Yilmaz, Ö., 1987, Seismic data processing: Society of Exploration Geophysicists. Tulsa, OK.

Appendix A

Radial components for synthetic seam models

In addition to the transverse component discussed in Chapter 4, the P- and SV- components (pseudo-Rayleigh seam wave) at a distance of 220 m were also computed. The pseudo-Rayleigh seam wave dispersion characteristics are much more complicated than those for the Love seam wave (refer to the figures below and Figures 4.9 and 4.11).

	$rock_1$ $coal$ $rock_1$	$rock_1$ $coal$ $rock_2$	$rock_1$ $coal/dirt/coal$ $rock_1$
V_{pr1} (m/s)	2000	2000	2000
V_{sr1} (m/s)	1400	1400	1400
ρ_{r1} (kg/m^3)	2200	2200	2200
V_{pr2} (m/s)	-	1600	-
V_{sr2} (m/s)	-	900	-
ρ_{r2} (kg/m^3)	-	1900	-
V_{pc} (m/s)	1200	1200	1200
V_{sc} (m/s)	700	700	700
ρ_c (kg/m^3)	1300	1300	1300
V_{pd} (m/s)	-	-	1300
V_{sd} (m/s)	-	-	900
ρ_d (kg/m^3)	-	-	1600

Table A.1: P and S (denoted by subscripts p and s) wave velocities and densities for the three tested layerstack models. Subscripts r1, r2, c and d denote values for $rock_1$, $rock_2$, *coal* and *dirtband* respectively. Velocities and densities obtained from Dombrowski et al. (1994).

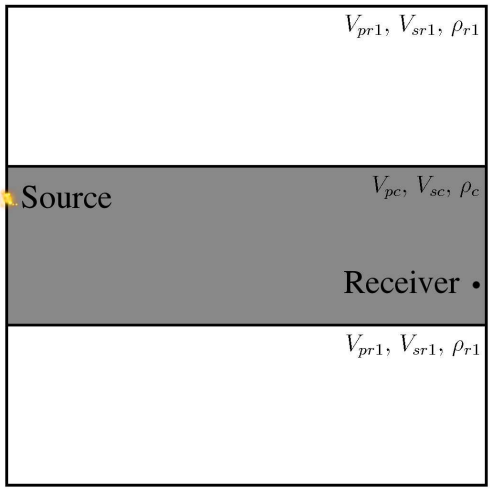

Figure A.1: Layerstack model for symmetric coal seam sequence.

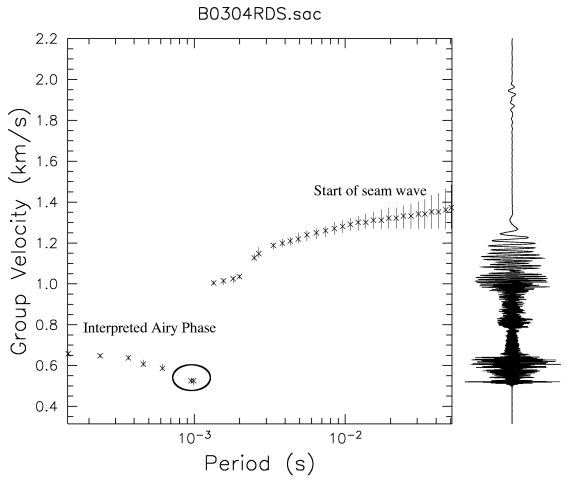

Figure A.2: Radial component for a dip-slip event.

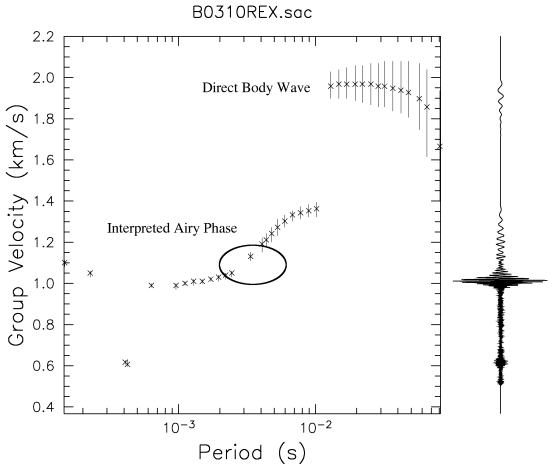

Figure A.3: Radial component for an explosion event.

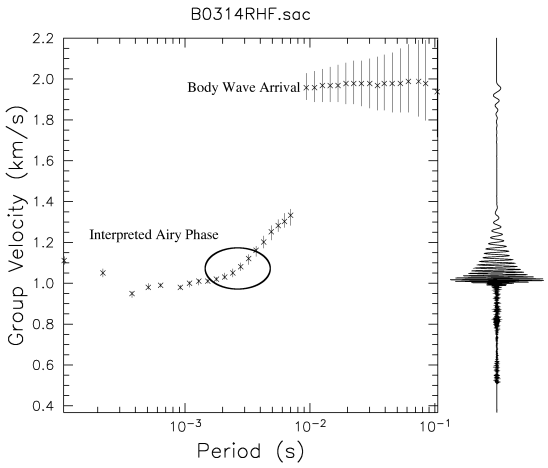

Figure A.4: Radial component for a horizontal point force.

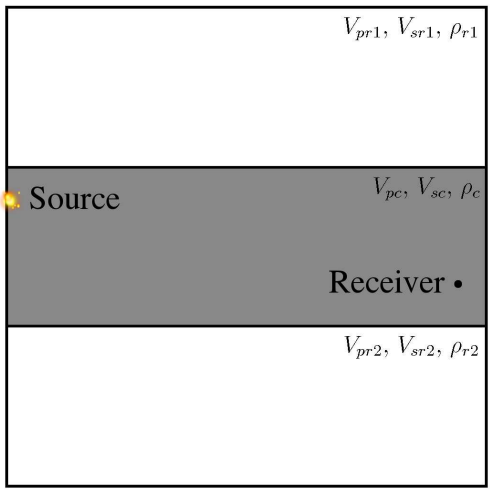

Figure A.5: Layerstack model for asymmetric coal seam sequence.

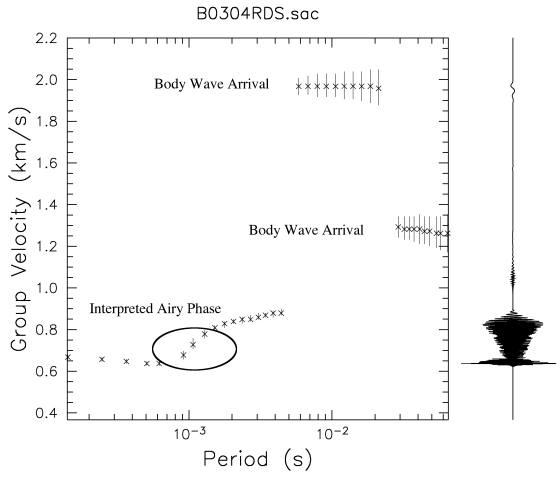

Figure A.6: Radial component for a dip-slip event.

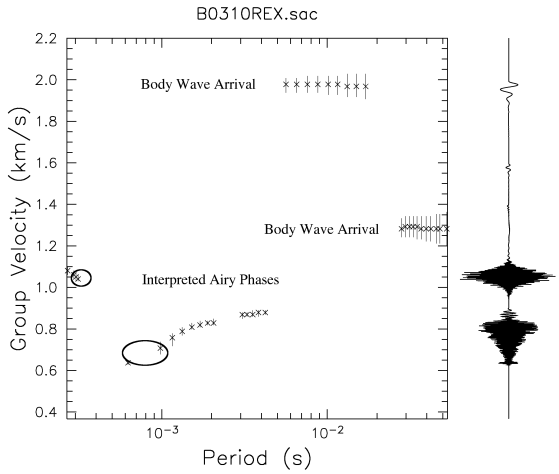

Figure A.7: Radial component for an explosion event.

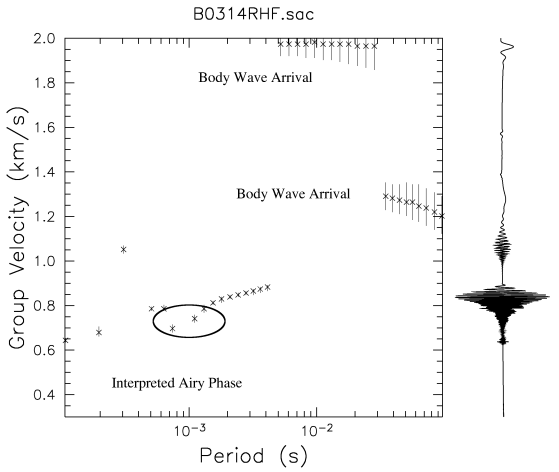

Figure A.8: Radial component for a horizontal point force.

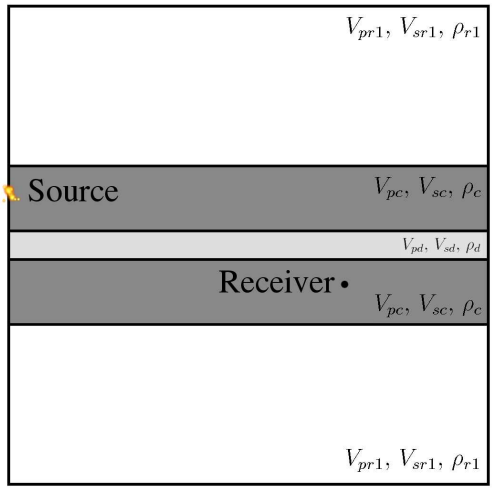

Figure A.9: Layerstack model for embedded dirband coal seam sequence.

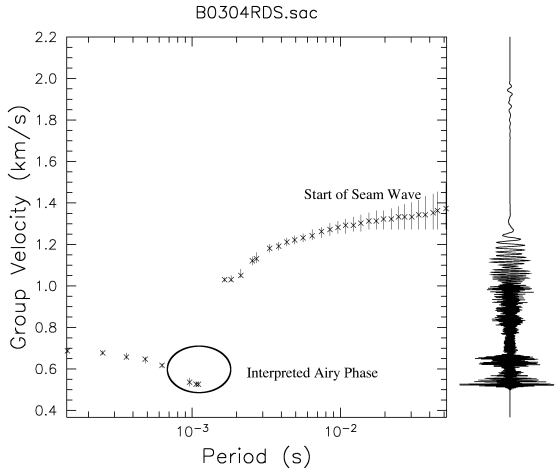

Figure A.10: Radial component for a dip-slip event.

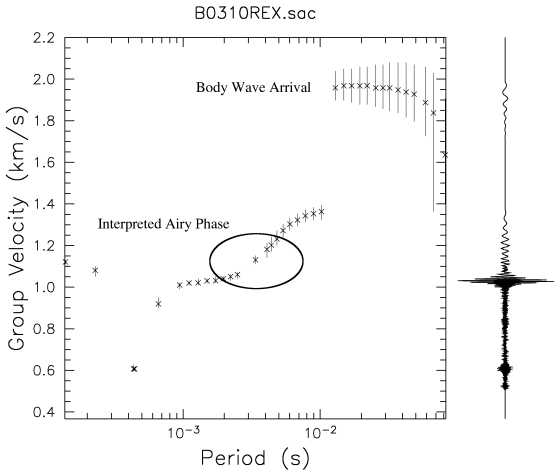

Figure A.11: Radial component for an explosion event.

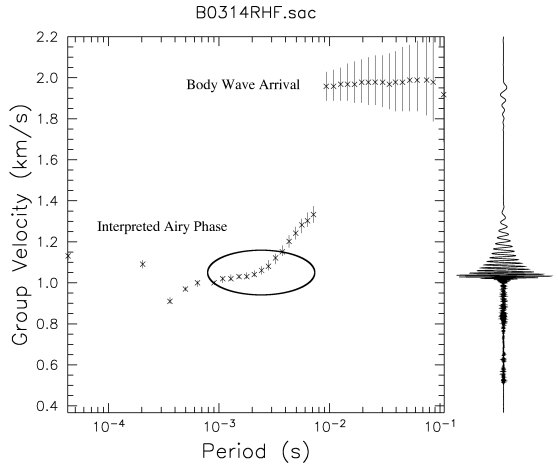

Figure A.12: Radial component for a horizontal point force.

Appendix B

Increasing seam wave thickness dispersion analysis

To gain understanding into frequency content and seam wave arrival times for seam models of varying thicknesses, synthetic traces for four symmetric models using the velocity and density values shown in the table below were computed by wavenumber integration. The seam models show a general trend of decreasing Airy phase frequency arrival as seam thickness increases (Table B.2).

	$rock_1$ $coal$ $rock_1$
V_{pr1} (m/s)	2000
V_{sr1} (m/s)	1400
ρ_{r1} (kg/m^3)	2200
I_{pr1} (kg/sm^2)	4400000
I_{sr1} (kg/sm^2)	3080000
V_{pc} (m/s)	1200
V_{sc} (m/s)	700
ρ_c (kg/m^3)	1300
I_{pc} (kg/sm^2)	1560000
I_{sc} (kg/sm^2)	910000

Table B.1: P and S (denoted by subscripts p and s) wave velocities, impedances, and densities for the symmetric coal seam layerstack model. Subscripts r1 and c denote values for $rock_1$ and *coal* respectively. Velocities and densities obtained from Dombrowski et al. (1994).

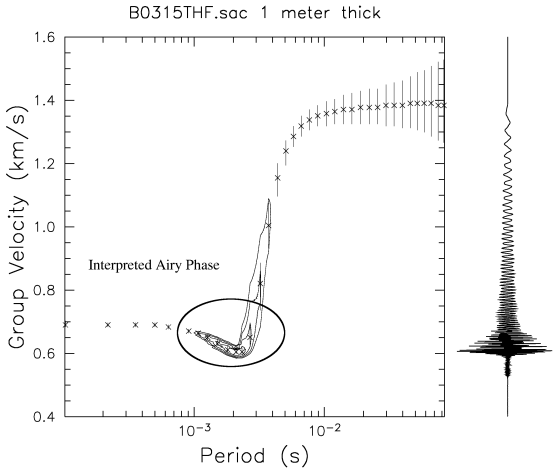

Figure B.1: Love seam wave dispersion for 1 m thick coal seam (data derived). Airy phase frequency 600–1100 Hz.

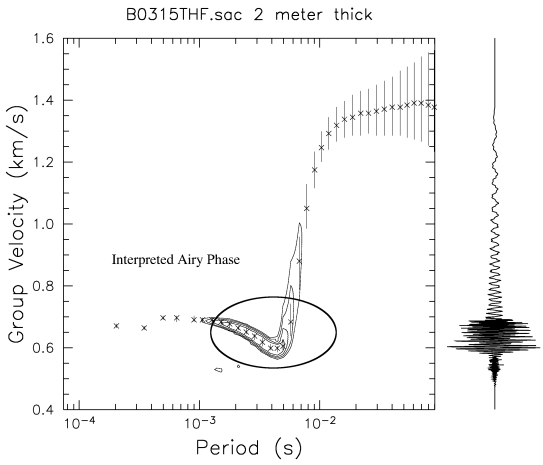

Figure B.2: Love seam wave dispersion for 2 m thick coal seam (data derived). Airy phase frequency 400–800 Hz

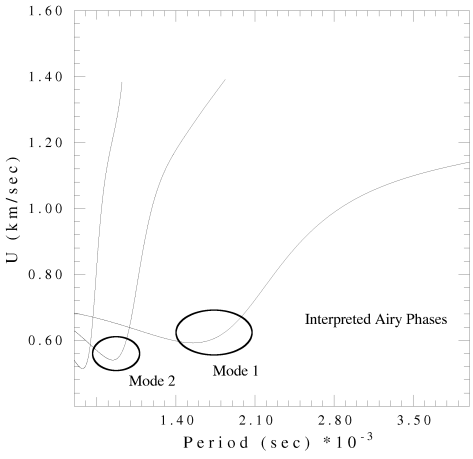

Figure B.3: Love seam wave dispersion for 3 m thick coal seam (theoretical). Airy phase frequency 100–500 Hz.

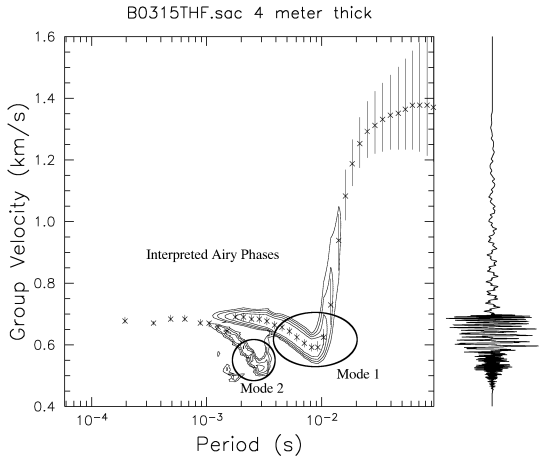

Figure B.4: Love seam wave dispersion for 4 m thick coal seam (data derived). Airy phase frequency 50–300 Hz.

Seam Thickness (m)	Frequency Range (Hz)	Seam Wave Velocity (m/s)
1	600-1100	500-700
2	400-800	500-700
3	100-500	500-800
4	50-300	500-800

Table B.2: Seam wave velocity and frequency content of Appalachian coal seams for different thicknesses

Appendix C

CPS modeling programs used for synthetic seismogram generation

All synthetic modeling was performed using the CPS modeling package created by Herrmann (2004).

Wavenumber integration workflow
hprep96 -M model.01 -d dist.file -HS 0.0001 -FHR rec.dep -ALL -TH -BH hspec96 hpulse96 -V -p -l 2 | fprof96

Table C.1: Wavenumber integration workflow

Analytic solution workflow
sprep96 -M model.01 -d dist.file -HS 0.0001 -FHR rec.dep -NMOD 3 -L -R sdisp96 slegn96 sregn96 sdpegn96 -L -R -U -C (note: specify one type at a time e.g. -L -U)

Table C.2: Analytic solution workflow